ADVANCES IN ATMOSPHERIC SCIENCES, VOL. 34, FEBRUARY 2017, 199–208

• **Original Paper** •

Preliminary Study on Direct Assimilation of Cloud-affected Satellite Microwave Brightness Temperatures

Sibo ZHANG and Li GUAN*

Collaborative Innovation Center on Forecast and Evaluation of Meteorological Disasters, Key Laboratory for Aerosol–Cloud–Precipitation of China Meteorological Administration, Nanjing University of Information Science and Technology, Nanjing 210044*, China*

(Received 21 February 2016; revised 13 May 2016; accepted 19 May 2016)

ABSTRACT

Direct assimilation of cloud-affected microwave brightness temperatures from AMSU-A into the GSI three-dimensional variational (3D-Var) assimilation system is preliminarily studied in this paper. A combination of cloud microphysics parameters retrieved by the 1D-Var algorithm (including vertical profiles of cloud liquid water content, ice water content, and rain water content) and atmospheric state parameters from objective analysis fields of an NWP model are used as background fields. Three cloud microphysics parameters (cloud liquid water content, ice water content, and rain water content) are applied to the control variable. Typhoon Halong (2014) is selected as an example. The results show that direct assimilation of cloud-affected AMSU-A observations can effectively adjust the structure of large-scale temperature, humidity and wind analysis fields due to the assimilation of more AMSU-A observations in typhoon cloudy areas, especially typhoon spiral cloud belts. These adjustments, with temperatures increasing and humidities decreasing in the movement direction of the typhoon, bring the forecasted typhoon moving direction closer to its real path. The assimilation of cloud-affected satellite microwave brightness temperatures can provide better analysis fields that are more similar to the actual situation. Furthermore, typhoon prediction accuracy is improved using these assimilation analysis fields as the initial forecast fields in NWP models.

Key words: atmospheric sounding, microwave remote sensing, data assimilation, cloudy radiances, GSI

Citation: Zhang, S. B., and L. Guan, 2017: Preliminary study on direct assimilation of cloud-affected satellite microwave brightness temperatures. *Adv. Atmos. Sci.*, **34**(2), 199–208, doi: 10.1007/s00376-016-6043-9.

1. Introduction

Satellite data assimilation systems employ a radiative transfer model to simulate radiative brightness temperatures from satellite observations. Excluding scattering effects from cloud and rain particles in the radiative transfer model severely restricts the simulation accuracy of cloud- or precipitation-affected satellite brightness temperatures. Hence, only clear-sky and partly non-precipitating cloudy satellite data can be assimilated into a data assimilation system. Gradual improvement of simulation abilities for cloud and precipitation areas' satellite radiances by the radiative transfer model provides an opportunity and a platform for assimilation of satellite observations over cloud and rain regions. In 2005, NASA, NOAA and the Department of Defense Joint Center for Satellite Data Assimilation (JCSDA) jointly launched an international seminar (the first of its kind) on satellite data assimilation over cloud and rain areas and noted that satellite work on visible, infrared and microwave bands can detect observations associated with clouds and precipitation (Errico et al., 2007). However, it was unclear how to use these observations to improve initial values of cloud and precipitation areas for NWP models, and this issue formed the focus of subsequent research. The next of these seminars took place in the spring of 2010, organized by the ECMWF and JCSDA (Ohring and Bauer, 2011). The ECMWF proposed a 1D+4D-Var (one-dimensional and four-dimensional variational) scheme to assimilate microwave imaging observations affected by precipitation, and presented the quality control method of retrieved parameters, the deviation correction scheme, and the definition of a formula for observation errors (Bauer et al., 2006a, 2006b). In 2010, the direct assimilation of all-weather satellite microwave imager sensor data in a 4D-Var data assimilation system was successfully carried out by the ECMWF (Bauer et al., 2010; Geer et al., 2010).

Currently, only clear-sky satellite observations are assimilated into the operational Global and Regional Assimilation and Prediction Enhanced System (GRAPES) in China. There is still a lack of studies on satellite data assimilation under cloudy conditions; only a few preliminary investigations

* Corresponding author: Li GUAN
Email: liguanlily@189.cn

with cloud-affected satellite infrared data assimilation have been carried out (Ding et al., 2009, 2010a, 2010b). To effectively assimilate cloud-affected satellite microwave observations, the primary problem involves improving the brightness temperature simulation abilities of radiative transfer models on cloud-area microwave observations. Using the rapid Community Radiative Transfer Model (CRTM), the radiative effect of water content on simulations of satellite microwave observations in cloudy and rainy areas was analyzed by Dong et al. (2009). The hydrometeor content input of CRTM was taken from the output of the regional mesoscale WRF model. Yang et al. (2012) studied the impact of directly assimilating clear-sky FY-3A microwave sounder data on typhoon numerical prediction. The simulation results of microwave satellite observations in the Typhoon Luosha (2007) area from both RRTMs, RTTOV and CRTM, were compared by Liu et al. (2012). It was shown that the characteristics of the response function and the influence on the simulation of satellite brightness temperatures of hydrometeors, were almost the same for RTTOV and CRTM. The simulated brightness temperature of CRTM was slightly larger than that of RTTOV. Meanwhile, FY-3A clear-sky microwave data assimilation and brightness temperature simulation under cloudy and rainy conditions were investigated by Dong et al. (2014).

Most satellite data assimilation research in China continues to focus on clear-sky data assimilation and cloudy-sky brightness temperature simulation. Much less and only preliminary research has taken place on direct assimilation of cloud-affected microwave data, although information obtainable from cloud and rain data has the potential to reduce the bias caused by cloud and rain for the NWP first guess fields. The purpose of the present study is to carry out direct assimilation, not only with clear-sky but also with cloud-affected satellite microwave brightness temperatures. Retrieved hydrometeor profiles from a 1D-Var algorithm [details can be found in Zhang et al. (2015)] and other atmospheric state parameters from objective analysis fields are taken as background input parameters for the 3D-Var GSI data assimilation system.

2. Data used for assimilation

Both satellite microwave imager and microwave sounder observations are used in this paper to realize direct assimilation of cloud-affected satellite microwave observations. AMSR-2 was installed on the GCOM-W1 (Global Change Observation Mission 1st-Water) satellite launched in 2012. It has a passive remote sensing sensor and is designed to detect cloud and earth surface parameters. AMSR-2 is the successor to AMSR-E, with 14 channels at the following seven microwave frequencies: 6.925 GHz, 7.3 GHz, 10.65 GHz, 18.7 GHz, 23.8 GHz, 36.5 GHz, and 89 GHz. These frequencies are window channels, except for 23.8 GHz in the weaker water vapor absorption region. Each frequency contains both horizontal and vertical polarizations. The microwave imager scans the earth conically with a constant earth incidence angle of 55° and a swath of 1445 km. As it orbits Earth in a sun-synchronous mode, its equator crossing times are 0130 LST and 1330 LST in its descending and ascending modes, respectively. The microwave imager onboard a meteorological satellite is primarily designed to enhance the sensing capabilities of cloud-water and cloud-ice content. In this study, AMSR-2 observations are used to retrieve hydrometeor profiles based on a 1D-Var algorithm.

AMSU-A is a cross track-scanning radiometer with a swath width of 2250 km for a total of 15 channels. It scans ±48.3° from the nadir, with a total of 30 Earth fields-of-view per scan line. Channels 1, 2, 3 and 15 of AMSU-A work at microwave window frequencies with central frequencies at 23.8 GHz, 31.4 GHz, 50.3 GHz and 89.0 GHz, respectively. These window channels are primarily used to detect cloud liquid water content and total column precipitable water content. The other 11 channels, with central frequencies from 52.8 GHz to 57.3 GHz, located at an oxygen absorption band, are sensitive to atmospheric temperature profiles. AMSU-A satellite observations have been proven to be highly effective for NWP because they enable it to detect not only atmospheric temperature and humidity profiles under clear-sky conditions, but also the internal structures of typhoons under cloudy and rainy conditions (Cardinali, 2009; Singh et al., 2012). Hence, in this study, AMSU-A observations are selected to explore the direct assimilation of cloud-affected microwave satellite data.

3. GSI 3D-Var data assimilation system

The GSI data assimilation system is used in this study because of its ability to assimilate data from many different observational platforms, including brightness temperatures obtained from satellites. It is a 3D-Var data assimilation system developed by NOAA that is used operationally at NCEP. Its predecessor is the Spectral Statistical Interpolation (SSI) system. The GSI system combines global and regional data assimilation models, primarily designed for regional forecasts, global forecasts, hurricane forecasts, real-time mesoscale analysis, and fast weather update forecasts (Kleist et al., 2009). The principal of GSI 3D-Var is to resolve the data assimilation problem into the minimization problem of the cost function, which represents the distance between the analysis field and model forecast field and the distance between the analysis field and observation field, based on the background data, observation data and their corresponding statistical error matrix. Thus, the 3D-Var analysis field is the solution when the objective function reaches a minimum value:

$$J = \frac{1}{2}(\boldsymbol{x}-\boldsymbol{x}_\mathrm{b})^\mathrm{T}\boldsymbol{B}^{-1}(\boldsymbol{x}-\boldsymbol{x}_\mathrm{b}) + \frac{1}{2}(\boldsymbol{y}_\mathrm{o}-\boldsymbol{H}(\boldsymbol{x}))^\mathrm{T}(\boldsymbol{O}+\boldsymbol{F})^{-1}(\boldsymbol{y}_\mathrm{o}-\boldsymbol{H}(\boldsymbol{x})) + J_\mathrm{c}\,, \quad (1)$$

where $\boldsymbol{x}$ is an analysis field, $\boldsymbol{x}_\mathrm{b}$ is a background field usually composed of values taken from a previous forecast, $\boldsymbol{y}_\mathrm{o}$ represents the observation data—in this case, of the satellite

data assimilation—and $\boldsymbol{y}_o$ is the satellite observed brightness temperatures. $\boldsymbol{H}$ is the observation operator, which transforms the model variables ($\boldsymbol{x}$) into the variables in the observation space. $\boldsymbol{H}$ contains a fast radiative transfer model (e.g., CRTM), which simulates measured brightness temperatures based on the atmospheric state $\boldsymbol{x}$ from the NWP model, as well as a temporal and spatial interpolation model for the satellite data assimilation. Additionally, $\boldsymbol{B}$ is the estimated error covariance matrix of the background field, $\boldsymbol{O}$ is the error covariance matrix from the observation instrument, $\boldsymbol{F}$ is the error covariance matrix from the accuracy of the operator, and J_c represents the constraint item. J_c includes two terms, one being the weak moisture constraint ($q > 0$, $q < q_{sat}$) and the other being the conservation of global dry mass. The first item in Eq. (1) represents the distance between the analysis field and the background field; the second item represents the distance between the analysis field and the observation field; and the third item is the constraint item. Furthermore, the assimilation analysis field $\boldsymbol{x}$ (namely, the initial field of the numerical prediction model, which is closer to actual observations) can be derived by making the cost function J a minimization using the iteration method. Subsequently, the forecast accuracy of the numerical forecast model can be enhanced.

When the cloud-affected AMSU-A observations are assimilated into the system, the observation operator errors under cloudy-sky conditions are higher than the clear-sky errors because the simulation capabilities of the observation operator in cloudy sky are not as good as those in clear sky. The observation operator errors in this paper are listed in Table 1.

Table 1. Observation operator errors for AMSU-A in the GSI system.

	Observation operator errors	
AMSU-A channel	Clear-sky (K)	Cloud-sky (K)
1	3.000	9.100
2	2.000	13.500
3	2.000	7.100
4	0.600	1.300
5	0.300	0.550
6	0.230	0.230
7	0.250	0.195
8	0.275	0.232
9	0.340	0.235
10	0.400	0.237
11	0.600	0.270
12	1.000	0.385
13	1.500	0.520
14	2.000	1.400
15	3.000	10.000

4. Assimilation experiment design and results analysis

Owing to the low accuracy of the hydrometeor information from the 6-h WRF forecast in the assimilation background field, brightness temperatures over cloudy areas are simulated as clear areas. This leads to a strong bias between simulated and actual observed brightness temperatures under cloudy conditions. As a result, the GSI system will directly discard observations associated with clouds. Through comparison we believe the hydrometeor profiles forecasted by WRF are less accurate than from the 1D-Var retrievals. So, the hydrometeor profiles are retrieved firstly by the 1D-Var method, then combined with other atmospheric state parameters as background fields. The first guess departure bias will decrease by considering the cloudy scattering effect with respect to clear-sky simulation, so more observations can be assimilated into system. Three cloud microphysics parameters (cloud liquid water content, ice water content, and rain water content) are added to the control variable in the variational assimilation process.

These cloudy observations with less first guess departure bias can partly pass the quality control of the GSI system and are directly assimilated into the system. Atmospheric temperature, humidity and wind fields are gradually adjusted using the inner iteration loop of the assimilation process, which leads to better agreement of the assimilation analysis field and satellite microwave observations.

The profiles of the three hydrometeors—cloud liquid water, cloud ice, and rainwater content—retrieved from the 1D-Var algorithm from AMSR-2 observations over the areas of Typhoon Halong (2014) on 4 August 2014, are added as inputs for the GSI background field to directly variationally assimilate space-borne cloudy AMSU-A observations. To validate the assimilation effect of cloudy-area microwave radiances, three groups of experiments are designed. In the control run (CNT), only conventional observations are assimilated; in experiment 1 (EXP1), conventional and clear-sky AMSU-A observations are assimilated; and in experiment 2 (EXP2), conventional and all-weather AMSU-A observations are assimilated. NCEP reanalysis fields with a $1^\circ \times 1^\circ$ resolution are used as boundary conditions and the initial fields of the WRF model in all the three tests. The 6-h forecast fields from the WRF model provide the background field for CNT and EXP1. In EXP2, these 6-h forecast atmospheric state parameters and the retrieved hydrometeors are composed of the background field. In our study, two assimilation cycles are carried out, at 0600 UTC and 1800 UTC, with an interval time of 12 h according to the temporal resolution of the AMSU-A observations.

First, the brightness temperatures from the AMSR-2 10.65 GHz vertical polarization observations are shown, in Fig. 1a. The warm colored pixels indicate the location and coverage areas of Typhoon Halong (2014). The total column content of the hydrometeors retrieved from 1D-Var are shown in Figs. 1b–d. The coverage areas with higher total content of cloud liquid water (Fig. 1b) within Halong are limited and mainly concentrated in the northwestern and southwestern parts of the typhoon spiral cloud belt. The major areas of the

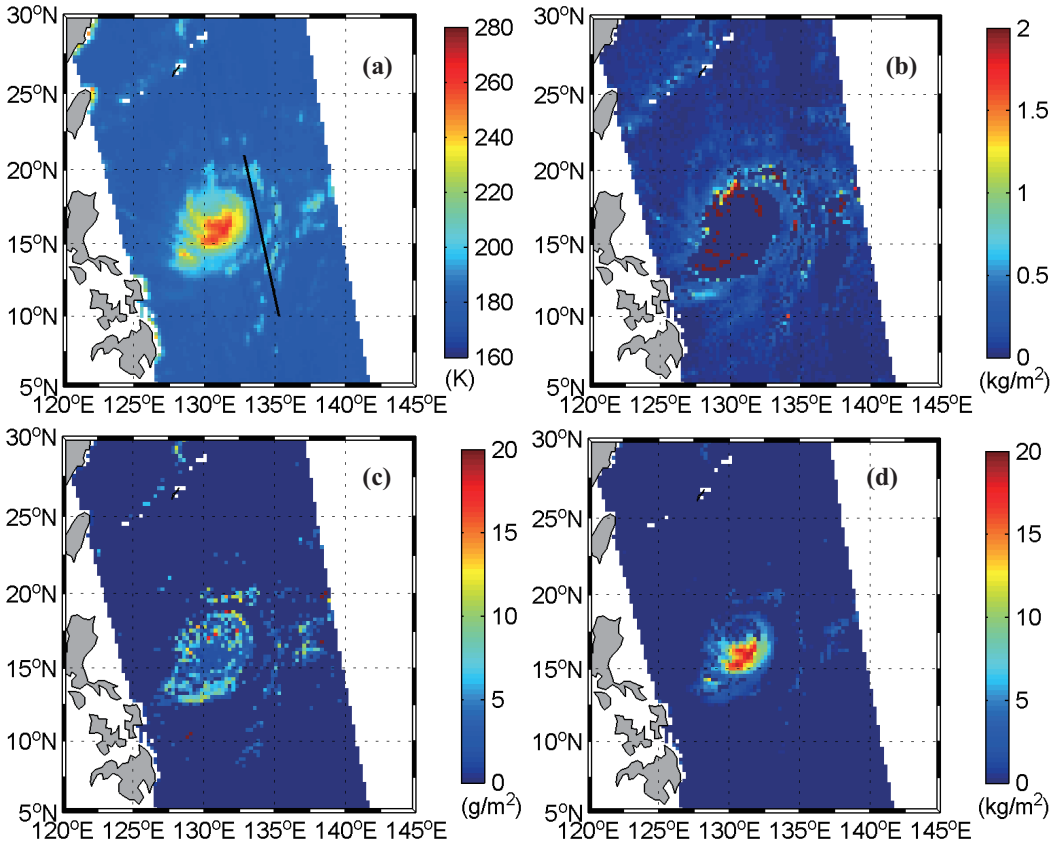

Fig. 1. Typhoon Halong (2014) on 4 August 2014: (a) AMSR-2 observations in the 10.65 GHz vertical polarization channel (the black line represents the flight track of CloudSat), and retrieved total content of (b) cloud liquid water, (c) cloud ice water and (d) precipitation, from the 1D-Var algorithm.

typhoon have higher cloud-ice content, as shown in Fig. 1c. The areas with higher cloud-ice content represent the cloud with higher tops or cirrus clouds. The position and strength distribution of the retrieved total rain content (Fig. 1d) are in good agreement with those of observed areas with higher brightness temperatures in Fig. 1a. Note that all the retrieved cloud liquid water, cloud ice water and rain contents in the observed typhoon regions are very high, which indicates that the hydrometeor parameters over typhoon areas could be retrieved successfully using the 1D-Var algorithm.

In addition to the total horizontal content of the retrieved hydrometeors, the vertical profiles of these hydrometeors are also analyzed to further validate the precision of the 1D-Var method. The radar reflectivity factor products (2B-GEOPROF) of the Cloud Profiling Radar (CPR) installed on the CloudSat satellite are used in Fig. 2 as reference for comparison with the vertical profiles of the retrieved hydrometeors. The black line in Fig. 1a represents the flight track of CloudSat. There are three obvious cloud streaks between 12°N and 16°N along this track, and an additional cloud streak near 18°–20°N with higher brightness temperatures. The echo of cloud radar along the black line is shown in Fig. 2a. Most of the radar reflectivity echoes are below 16 km. The regions with intense echo are in good agreement with the typhoon cloud belts (Fig. 1a), especially the cloud areas with higher echo tops and stronger reflectivity close to 14°N and 18°–20°N. The vertical profiles of rain water content and cloud water content retrieved from the 1D-Var algorithm are shown in Figs. 2b and c. The pixels with retrieved hydrometeor content at high levels match the distribution of the CloudSat CPR strong echo well, which indicates that the vertical profiles of hydrometeors over cloud areas can be correctly retrieved. There is an approximate 18-min time difference between the AMSR-2 observation scanned at 0405 UTC in the ascending node and the CPR echo measured at 0347 UTC on 4 August 2015. The sampling spatial resolution is also different. The horizontal resolution for AMSR-2 is 62 km ×35 km, which is much larger than the resolution of the CPR observations (2.5 km ×1.4 km). These discrepancies in time and space may lead to variance when comparing the two observations.

In our earlier study (Zhang et al., 2015), CRTM-simulated brightness temperatures over Typhoon Halong (2014) areas under clear-sky and cloudy-sky conditions were compared. The hydrometeor profiles retrieved from the 1D-Var algorithm complemented the radiative transfer model (observation operators), in which cloud absorption and scattering effects were considered. Simulated and observed brightness temperatures showed good agreement for all AMSR-2 microwave channels. The shape, intensity and

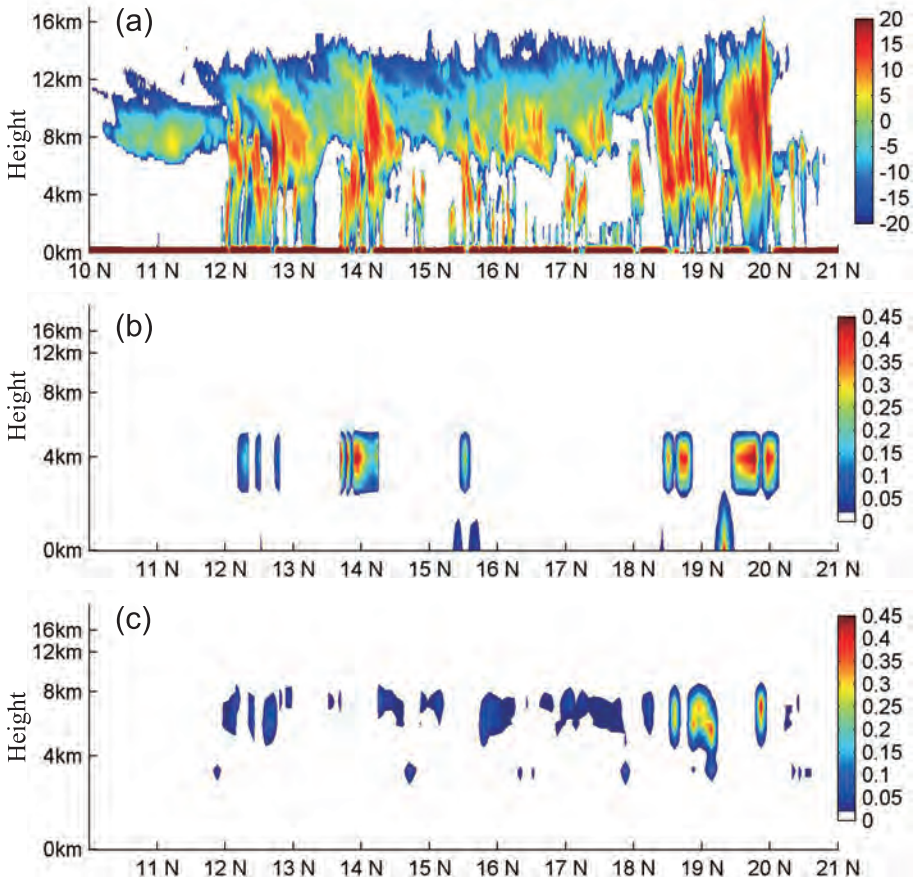

Fig. 2. The vertical profiles of (a) CPR reflectivity echo (dBZ), (b) retrieved rain water (kg m^{-2}), and (c) retrieved cloud water (kg m^{-2}), on 4 August 2014.

spiral structure of the typhoon could be described well. The departures between the simulations with retrieved hydrometeors and the observations were significantly lower than the departures between the clear simulations without retrieved hydrometeors and the observations. The improvements in the simulations of the brightness temperatures over the typhoon areas also indicated that the precision of hydrometeor retrievals from the 1D-Var algorithm is very high.

The GSI bias correction algorithm and quality control scheme for all AMSU-A channels are completely retained in EXP1 and EXP2. The bias between the observations and simulations in EXP2 without scan angle and air mass bias correction (Fig. 3a) and with bias correction (Fig. 3b) at 0600 UTC 4 August 2015, is shown in Fig. 3. The observations with a bias between the simulation from the background field and the observations larger than the threshold will be rejected by the quality control of the assimilation system. The quality control thresholds in the AMSU-A window channels over cloud areas are larger than over clear sky; for example, 9.1 K for 23.8 GHz, 13.5 K for 31.4 GHz, 7.1 K for 50.3 GHz, and 10 K for 89.0 GHz. For other channels with less cloud impact, the thresholds are set to less than 1.5 K. Taking the 23.8 GHz window channel as an example, the distribution of all observations passed the GSI's quality control, and the corresponding bias between the simulations from the background field and the observations for EXP1 is shown in Fig. 4a.

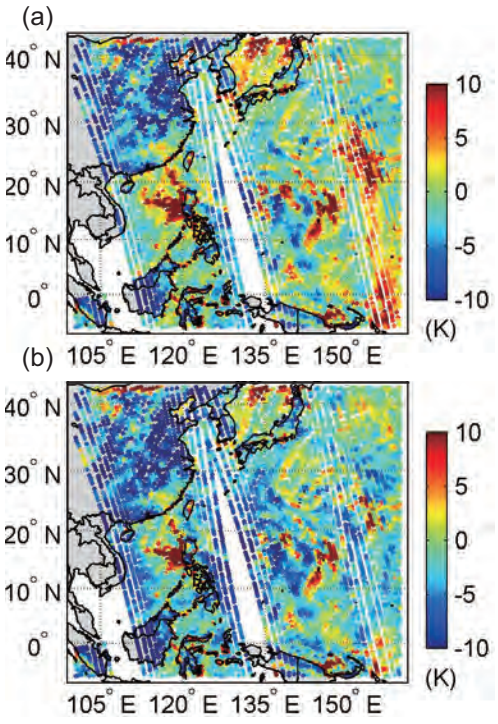

Fig. 3. The bias between observations and simulations in EXP2, (a) without bias correction and (b) with bias correction, at 0600 UTC 4 August 2014.

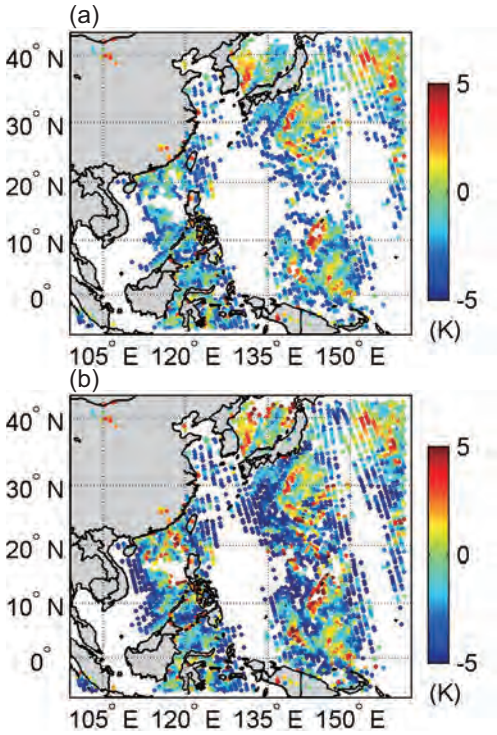

Fig. 4. The positions of AMSU-A 23.8 GHz observations that passed the quality control, and the bias between observations and simulations of (a) EXP1 and (b) EXP2, at 0600 UTC 4 August 2014.

Figure 4b is similar, except for EXP2. The rejection of the observations over the eye region could be due to the fact that the model-simulated cyclone eye is dislocated compared to the observed eye. It can be seen that EXP2 is able to assimilate more observations than EXP1, especially in the typhoon spiral cloud bands. However, assimilated observations over the typhoon eye area are still sparse because the microwave penetration ability is limited in multi-layer clouds or very dense cloud areas. When the cloud water content reaches a certain value, observation brightness temperatures for each channel no longer increase with increasing cloud water. They tend to be uniform, known as "observation-saturated", which restricts the precision of the hydrometeors retrieved from passive microwave remote sensing data. Due to the complexity of microwave passive detection, the bias between the simulations from the radiative transfer model and the observations is still large over dense cloud areas, leading to these observations being discarded by the data assimilation system.

To illustrate the structure of the increments imposed on the model field by the assimilation of AMSU-A radiances at 0600 UTC 4 August 2015, the 200-hPa temperature analysis field for CNT is shown in Fig. 5a. Figure 5b gives the temperature difference between EXP1 minus CNT, and Fig. 5c describes the temperature difference of EXP2 minus CNT. The warm core of the typhoon is clearly revealed in Fig. 5a. There is a slight warming (approximately 0.1 K) over the warm core at high altitude in EXP1 (Fig. 5b). In contrast, a cooling (approximately 0.2 K) is shown in Fig. 5c for EXP2, which is due to an intensity reduction of the 200-hPa typhoon warm core. Figure 6 displays the vertical section of the temperature analysis field along 17°N (crossing the typhoon center) in EXP2 (Fig. 6a) and EXP2 minus CNT (Fig. 6b). The structure of the typhoon warm core is very clear until 200 hPa in Fig. 6a. Compared to CNT, the temperatures of warm core areas at lower levels are decreased in EXP2. The weakened warm core reduces the intensity of the typhoon center, which correlates with the actual typhoon intensity variation, from 945 hPa at 0600 UTC to 950 hPa at 1800 UTC.

The low-level temperature and humidity analysis fields at 850 hPa in CNT, EXP1 and EXP2 are displayed in Fig. 7. The 850-hPa temperature analysis field is shown in Fig. 7a, and Fig. 7d illustrates the water vapor mixing ratio analysis field for CNT. The temperatures are higher in the center than in the peripheral spiral cloud bands. Humidities are also higher in the center of the typhoon and in the spiral cloud bands in CNT. The temperature difference fields in Fig. 7b (EXP1 minus CNT) and Fig. 7c (EXP2 minus CNT), and the

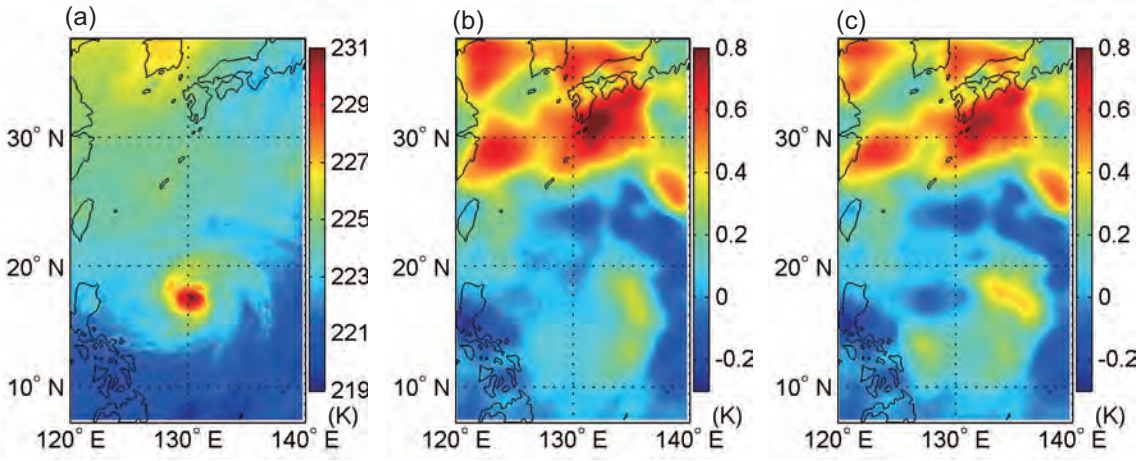

Fig. 5. The 200-hPa temperature analysis field at 0600 UTC 4 August 2014 in (a) CNT, (b) EXP1 minus CNT, and (c) EXP2 minus CNT.

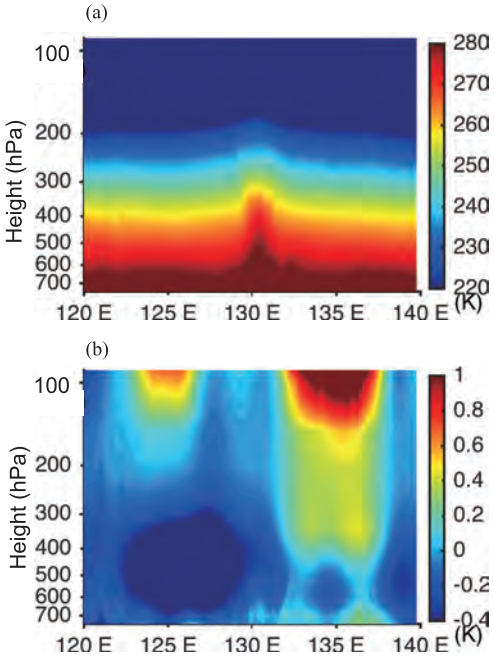

Fig. 6. Vertical section of the temperature analysis field along 17°N in (a) EXP2 and (b) EXP2 minus CNT.

water vapor mixing ratio difference fields in Fig. 7e (EXP1 minus CNT) and Fig. 7f (EXP2 minus CNT), indicate that there are more notable temperature and humidity field adjustments in EXP2, especially in the typhoon spiral cloud bands. Whereas a warming and drying phenomenon is present in the southern part of the typhoon, with thicker and higher cloud, cooling and wetting is revealed for the northwest and northeast areas of the typhoon periphery, with sparse and shallow cloud. In summer, typhoons form from low-latitude regions of the western Pacific, which are affected by the easterly flow from the southern part of the subtropical high of the western Pacific. There are three main types of moving path: westward, northwest, and turning northeast (Qian, 2004). In the assimilation analysis field of EXP2, a cooling phenomenon in the western and eastern parts of the typhoon can be observed. Notable warming is detected only in the north-northwestern part of the typhoon. Based on the fact that typhoons tend to move towards warm areas, the typhoon is more likely to move to the north-northwest in EXP2, which coincides with the actual typhoon's movement provided by the Shanghai Typhoon Institute (figure omitted).

For a successful data assimilation case, analysis departures between observation brightness temperatures and assimilation analysis field simulations should be smaller than

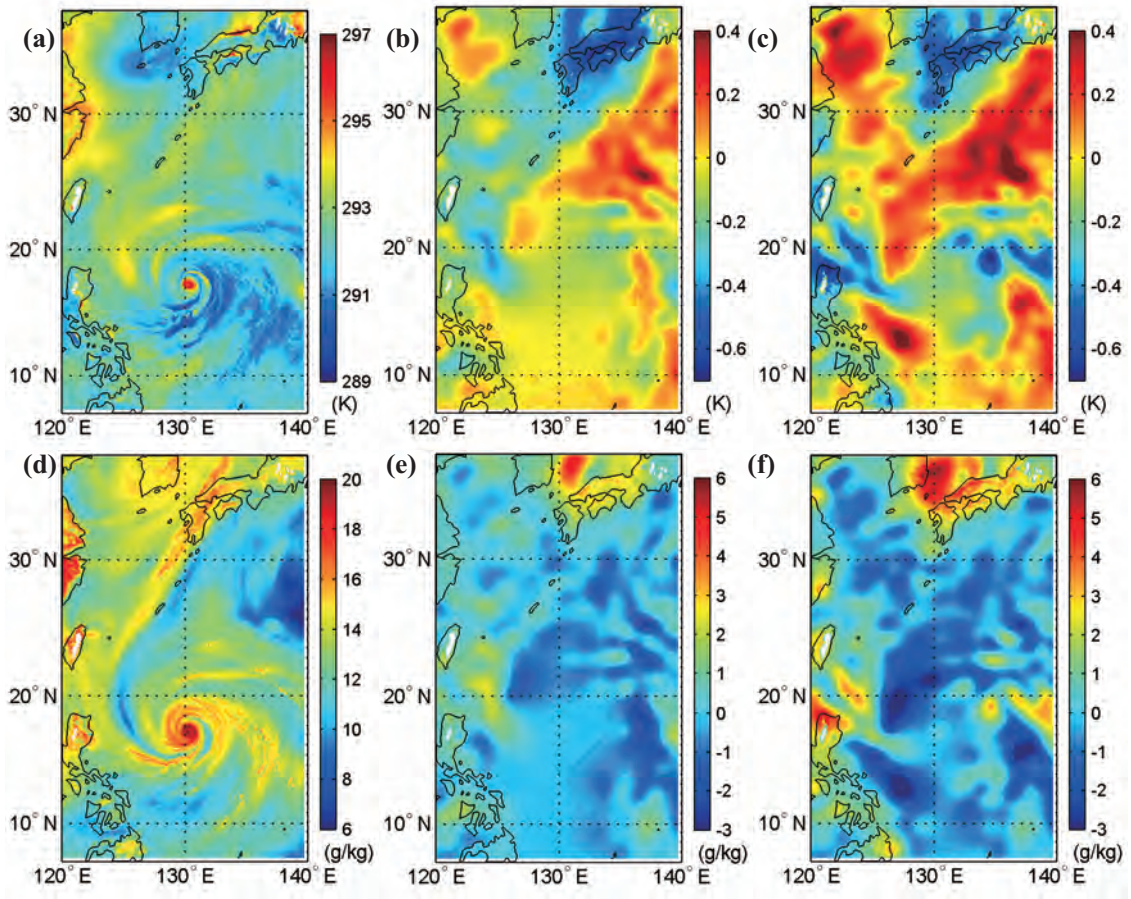

Fig. 7. The 850-hPa temperature analysis field at 0600 UTC 4 August 2014 in (a) CNT, (b) EXP1 minus CNT and (c) EXP2 minus CNT; and the water vapor mixing ratio analysis field in (d) CNT, (e) EXP1 minus CNT and (f) EXP2 minus CNT.

first guess departures between observations and background field simulations, i.e., the analysis field should correlate better with satellite observations than with the model background field. The PDFs of analysis departure (solid line) and first guess departure (dashed line) in the 23.8 GHz window channel in EXP2 are illustrated in Fig. 8. The first guess departure ranges from −10 K to 6 K, whereas the analysis departure is greatly reduced after data assimilation. Furthermore, the RMSE of analysis departure (1.25 K) is significantly smaller than that of first guess departure (3.12 K). The analysis departure PDFs are more Gaussian-like and unbiased than those of first guess departure. The figures for other channels are similar and hence are not shown here. It can be concluded that after assimilation adjustments of atmospheric temperature and humidity, the analysis field coincides more with the actual satellite observations than with the background field.

Because AMSR-2 scans Earth once every 12 h, the second assimilation time is selected as 1800 UTC, 12 h after the first assimilation time. Atmospheric wind fields, typhoon intensity and position simulations in CNT, EXP1 and EXP2 are shown in Fig. 9. Figures 9a–c show the analysis wind field at 900 hPa shaded with an SLP field in CNT, EXP1 and EXP2, respectively. The typhoon center (17.94°N, 129.27°E) for CNT is approximately 62 km southwest of the best-track position (18.3°N, 129.7°E). For EXP1, the typhoon center (18.04°N, 129.38°E) is approximately 46 km from the best-track position, and the simulated typhoon center (18.04°N, 129.38°E) for EXP 2 is approximately 32 km away. Among the three experiments, the simulation of the typhoon's position in EXP2 is the closest to the actual data. Additionally, the observed minimum pressure near the typhoon center is 950 hPa, whereas the simulated values from CNT, EXP1 and EXP2 are 943.4 hPa, 944.8 hPa and 950.9 hPa, respectively. The typhoon central intensities of CNT and EXP1 are slightly (4–6 hPa) stronger than observed (950 hPa), whereas the intensity simulation from EXP2 is in better agreement with the actual observation due to the weakened warm core at 200 hPa. Thus, EXP2 can provide a better first guess field for NWP.

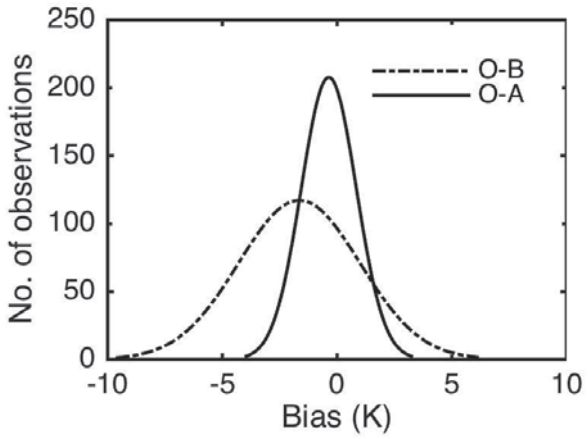

Fig. 8. Statistical distribution of analysis departures (O-A, solid line) and first guess departures (O-B, dashed line) for the AMSU-A 23.8 GHz observations in EXP2 at 0600 UTC 4 August 2014.

A 72-h weather forecast is made using the WRF model with the assimilation analysis at 1800 UTC as the initial forecast field. The double-nested domain of WRF is configured with a 30-km horizontal resolution parent domain with approximately 196×174 model grid points, and an inner domain at 10 km with approximately 193×316 grids. Both these domains are centered at (20°N, 130°E). The WRF model is configured with 31 vertical levels and a model top placed at approximately 50 hPa. The WSM6-class graupel scheme for microphysics, the New Kain–Fritsch cumulus convection parameterization scheme, and the YSU (Yonsei University) planetary boundary layer scheme are employed in the WRF atmospheric model in this study. The RRTM and Dudhia scheme are used for longwave and shortwave radiation, respectively. The predicted typhoon path is shown in Fig. 10. The black line is the actual typhoon path. The blue, green and red lines denote the predicted paths of CNT, EXP1 and EXP2, respectively, every 3 h. The results from EXP2 simulate the real path best, i.e., the assimilation scheme that best integrates conventional and all-weather AMSU-A observations. The assimilation of cloud-affected satellite

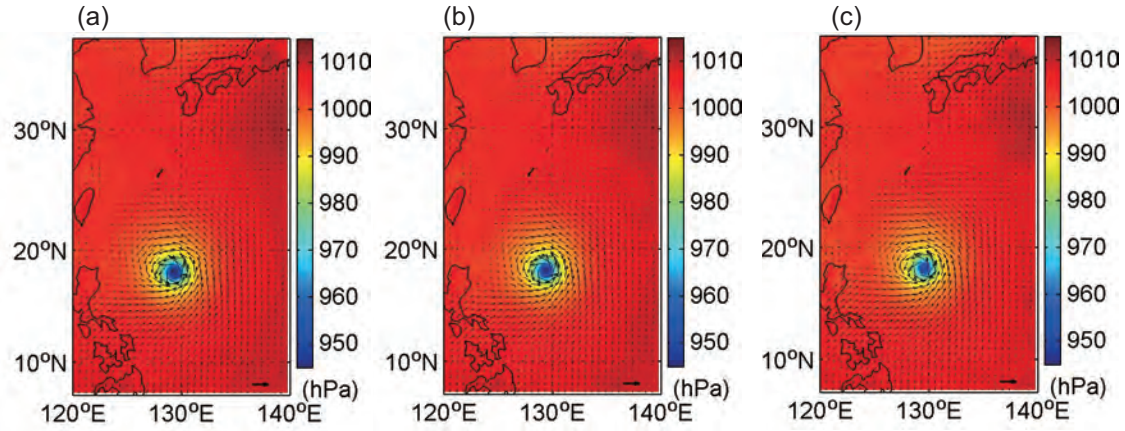

Fig. 9. The wind analysis field at 900 hPa (shaded with SLP) in (a) CNT, (b) EXP1 and (c) EXP2, at 1800 UTC 4 August 2014.

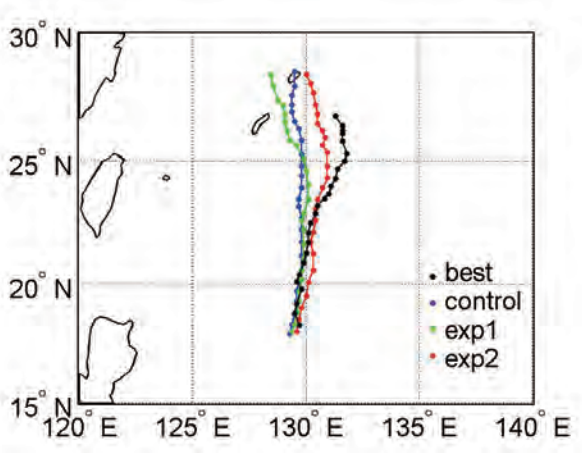

Fig. 10. The predicted path of Typhoon Halong (2014) from 1800 UTC 4 August to 1800 UTC 7 August 2014.

microwave brightness temperatures can provide better analysis fields, which are closer to the actual situation. Furthermore, the typhoon prediction accuracy can be improved by applying an NWP model using this assimilation analysis fields as initial forecast fields.

5. Conclusion

The direct assimilation of cloud-affected microwave brightness temperatures from AMSU-A into the GSI 3D-Var assimilation system is preliminarily studied in this paper. Adding the hydrometeor profiles retrieved by the 1D-Var algorithm to the background field of the data assimilation, which provides the initial values of the hydrometeors for the radiative transfer model, reduces the departures between the simulations and observations, leading to more cloudy-area satellite microwave observations being absorbed into the data assimilation system.

Taking Typhoon Halong (2014) at 0600 UTC and 1800 UTC 4 August 2014 during its mature stage as an example, we design three groups of assimilation experiments. For CNT, only conventional observations are assimilated; for EXP1, conventional and clear-sky AMSU-A observations are assimilated; and for EXP2, conventional and all-weather AMSU-A observations are assimilated, by the scheme proposed in this paper. The assimilation analysis fields are then analyzed and compared. It is found that EXP2 assimilates more AMSU-A observations into the data assimilation system than EXP1, especially satellite cloudy observations located in the typhoon peripheral spiral cloud bands. Adjustments to large-scale temperature, humidity and wind analysis fields by EXP2 relative to CNT and EXP1 confirm that the assimilation analysis field from EXP2 is closer to that of actual observations. Furthermore, typhoon prediction accuracy is improved by applying the NWP model, using the assimilation analysis fields as the initial forecast fields.

In future work it would be interesting to see if the assimilated cloud-affected satellite microwave observations can be extended to other instruments, such as AMSU-B/MHS, MWTS and MWHS, installed on the Chinese FY-3 satellite series. Direct assimilation of all-weather satellite microwave data will be carried out gradually in the operational data assimilation system.

Acknowledgements. The authors would like to thank the editor and reviewers for their helpful comments on the manuscript. This work was supported by the National Natural Science Foundation of China (Grant Nos. 41575029 and 41375106) and the Six Talent Peaks project of Jiangsu Province (Grant No. 2014JY021).

REFERENCES

Bauer, P., P. Lopez, D. Salmond, A. Benedetti, D. Salmond, and E. Moreau, 2006a: Implementation of 1D+4D-Var assimilation of precipitation-affected microwave radiances at ECMWF. I: 1D-Var. *Quart. J. Roy. Meteor. Soc.*, **132**, 2277–2306.

Bauer, P., P. Lopez, D. Salmond, A. Benedetti, S. Saarinen, and M. Bonazzola, 2006b: Implementation of 1D+4D-Var assimilation of precipitation-affected microwave radiances at ECMWF. II: 4D-Var. *Quart. J. Roy. Meteor. Soc.*, **132**, 2307–2332.

Bauer, P., A. J. Geer, P. Lopez, and D. Salmond, 2010: Direct 4D-Var assimilation of all-sky radiances. Part I: Implementation. *Quart. J. Roy. Meteor. Soc.*, **136**, 1868–1885.

Cardinali, C., 2009: Monitoring the observation impact on the short-range forecast. *Quart. J. Roy. Meteor. Soc.*, **135**, 239–250.

Ding, W. Y., Q. L. Wan, C. Z. Zhang, Z. T. Chen, and Y. Y. Huang, 2009: Modis brightness temperature data assimilation under cloudy conditions I—Methods and ideal tests. *Journal of Tropical Meteorology*, **25**, 649–659. (in Chinese)

Ding, W. Y., Q. L. Wan, Y. Y. Huang, Z. T. Chen, and C. Z. Zhang, 2010a: Modis brightness temperature data assimilation under cloudy conditions II—Impact on rainstorm forecasting. *Journal of Tropical Meteorology*, **26**, 22–30. (in Chinese)

Ding, W. Y., Q. L. Wan, C. Z. Zhang, Y. Y. Huang, and Z. T. Chen, 2010b: Assimilation of HIRS/3 brightness temperature in cloud condition and its impact on Typhoon Chanchu forecast. *Acta Meteorologica Sinica*, **68**, 70–78. (in Chinese)

Dong, P. M., H. J. Wang, W. Han, and D. Y. Wang, 2009: The effect of water content on the simulation of satellite microwave observation in cloudy and rainy area. *Journal of Applied Meteorological Science*, **20**, 682–691. (in Chinese)

Dong, P. M., J. P. Hang, G. Q. Liu, and T. Zhang, 2014: Assimilation of FY-3A microwave observations and simulation of brightness temperature under cloudy and rainy condition. *Journal of Tropical Meteorology*, **30**, 302–310. (in Chinese)

Errico, R. M., P. Bauer, and J. F. Mahfouf, 2007: Issues regarding the assimilation of cloud and precipitation data. *J. Atmos. Sci.*, **64**, 3785–3798.

Geer, A. J., P. Bauer, and P. Lopez, 2010: Direct 4D-Var assimilation of all-sky radiances. Part II: Assessment. *Quart. J. Roy. Meteor. Soc.*, **136**, 1886–1905.

Kleist, D. T., D. F. Parrish, J. C. Derber, R. Treadon, W.-S. Wu, and S. Lord, 2009: Introduction of the GSI into the NCEP global data assimilation system. *Wea. Forecasting*, **24**, 1691–1705.

Liu, S. S., P. M. Dong, W. Han, and W. J. Zhang, 2012: Simulative study of satellite microwave observations for Typhoon

Luosha using RTTOV and CRTM and the comparison. *Acta Meteorologica Sinica*, **70**, 585–597. (in Chinese)

Ohring, G., and P. Bauer, 2011: The use of cloud and precipitation observations in data assimilation (CPDA). *Quart. J. Roy. Meteor. Soc.*, **137**, 1933.

Qian, W. H., 2004: *Synoptic Meteorology*. Peking University Press, 210–230. (in Chinese)

Singh, R., C. M. Kishtawal, P. K. Pal, and P. C. Joshi, 2012: Improved tropical cyclone forecasts over north Indian Ocean with direct assimilation of AMSU-A radiances. *Meteor. Atmos. Phys.*, **115**, 15–34.

Yang, Y. M., M. B. Du, and J. Zhang, 2012: Experiments of assimilating FY-3A microwave data in forecast of typhoon MORAKOT. *Journal of Tropical Meteorology*, **28**, 23–30. (in Chinese)

Zhang, S. B., L. Guan, Y H. Li, and X. Y. Ren, 2015: The simulation of satellite microwave channels brightness temperature for cloudy areas. *Journal of Tropical Meteorology*, **31**, 664–672. (in Chinese)